EXPERIMENTAL INVESTIGATION ON THE PERFORMANCE OF A LITHIUM CHLORIDE WHEEL

A. A. Rabah

Department of Chemical Engineering, University of Khartoum, P. O. Box 321, Khartoum, Sudan.

Abstract

This work has investigated the influence of change in operation conditions on the performance of a Lithium Chloride (LiCl) wheel. A rigorous experimental rig that facilitates the measurement of temperature, pressure, pressure drop, relative humidity, airflow rate and rotational speed is used. The measurements covered balanced flow at a wide range of rotational speeds (0 - 9.8 rpm), regeneration temperatures (50 - 70 °C*), airflow rates (280-540* kg/h*) and relative humidities (30 -65%) at ambient condition. The influence of those operation conditions on the wheel sensible effectiveness and coefficient of performance (COP) are analyzed. The result revealed that a maximum COP occurs at a rotational speed of 0.2 rpm (12 rph). The results also concluded that Kays and London correlation is sufficient in the prediction of the effectiveness of the LiCl wheel. It represents the experimental data with an average absolute percent deviation (AAPD) of 2.16 and a maximum absolute percent deviation (APD_{max}) of about 6.00.*

Keywords: LiCl wheel, coefficient of performance, experimentation, effectiveness.

1 Introduction

Desiccant wheels are included in most heating, ventilation and air reconditioning (HVAC) designs for commercial buildings. The wheel consists of a matrix driven by a motor. The channels of the matrix can be of different configurations such as parallel surfaces, equilateral triangle, square, hexagonal, circular or corrugated geometry. The matrix may be made of metal coated with molecular sieves or silica gel or paper impregnated with lithium chloride (LiCl). The matrix, usually, has a large heat and mass transfer area per unit volume (e.g. 3000-4500 m^2/m^3) and a large number of channels per surface area of the face (e.g. 40,000 channels/m^2) [1]. The wheel is divided into two parts: one for process air and the other for the regeneration air. Water vapor of the process air is adsorbed and stored in the matrix. As the wheel rotates to the regeneration side the adsorbed water vapor is driven out by the hot regeneration air. Although LiCl wheel has short life, compared to Silica gel and molecular sieve, it has the advantage of low regeneration

temperature (≤70 °C). This characteristic make LiCl wheel more attractive for solar cooling where low regeneration temperature (< 70 °C) is available.

Although LiCl wheel has been developed in the 1970's, its disadvantage of short life has limited its application until recently. With recent advances in cellulose papers such as improvement in their lives and thermal characteristics, interest has been dawn again to LiCl wheels. Review of the catalogues of various HVAC desiccant wheels manufacturers', such as Klingenburg (Germany), Munsters (USA, Sweden), Seibu Giken (Japan), Proflute (Sweden) and DRI (India), to mention a few, confirms this trend.

In accordance with ANSI/ASHRAE [2] and ASHRAE Standard 84-2008 [3] the desiccant wheel performance is influenced by several operating parameters such as rotational speed, regeneration temperature, volumetric air-flow rate and inlet process air humidity and temperature. The are too many performance factors of the desiccant wheel. These include sensible (ε_s), latent (ε_l) and total (ε_t) effectiveness as one group. This set of performance factors is characteristic with the dimensionless parameters of airflow capacity (C^*), matrix heat capacity (Cr^*), matrix moisture capacity (Crm^*) and number of transfer units (NTU) to mention a few. The other groups of performance indices include moisture removal capacity (D), relative moisture removal efficiency (η) and latent (or dehumidification) coefficient of performance (COP).

The influence of operation conditions on the performance factors and performance indices has been studied by a number of researchers. Simonson and Besant [4], Simonson and Besant [5], Simonson and Besant [6], Simonson et al. [7] have published a series of papers covering both experimental and numerical investigation on molecular sieve and silica gel wheels. The main areas that are covered by their work include sensitivity analysis, parametric study and development of correlations for the prediction of desiccant wheel performance factors. Ge et al. [8] has developed a numerical model for the prediction of the performance factors of the desiccant wheel. The have recommended that the optimum operation conditions of the wheel are 2.0 to 3.5 m/s of process airflow rate, 2.5 to 3.5 m/s for regeneration airflow rate and an optimal rotational speed of 12 rph. Other numerical studies include the works of Xuan and Radermacher [9], Zheng and Worek [10] and Rabah and Mohammed [11].

It is clear that most of the available works are on the silica gel and molecular sieve wheels. Consequently, the main objective of this work is to study the influence of the operation conditions of rotational speed, regeneration temperature and airflow rate on the performance factors and indices of LiCl wheel. A

sophisticated experimental rig is developed which facilitates the measurement of operating conditions with a high accuracy.

2 Experimental setup

Figure 1 shows a schematic representation of the experimental setup. It consists of a desiccant wheel (D), an electric heater (H) and two sets of air fans (F1) and (F2) installed in a wind tunnel. The wind tunnel is insulated using Ampflex foam of 10 mm thickness. The desiccant is of type SECO 505/655-400 manufactured by Klingenburg. The wheel's matrix is made of paper impregnated with lithium chloride (LiCl). It is a 0.12 mm thickness with sine wave channels. Tab. 1 shows the specification of the wheel. The wheel is driven by a 90 W motor with variable frequency in the range of 0-120 Hz, equivalent to a rotational speed of 0-11 rpm. The motor regulator is of the type KR4R. The electric heater, manufactured by VOLTA, has a variable power of 0-7.2 kW. Four (4) air fans, connected in parallel, were used for each air stream. Each air fan has a power consumption of 100 W delivering an air volume of up to 200 m^3/h.

The LiCl wheel is operated in a counter current arrangement. For the regeneration section, ambient air is compressed using the air fans. Prior to the inlet of the LiCl wheel, the air is passed through the electric heater. This is made to bring the regeneration air to the desired temperature in the range of 40 to 100 °C. At the exit of the electric heater a distribution plate is installed to create a uniform temperature at the LiCl wheel inlet.

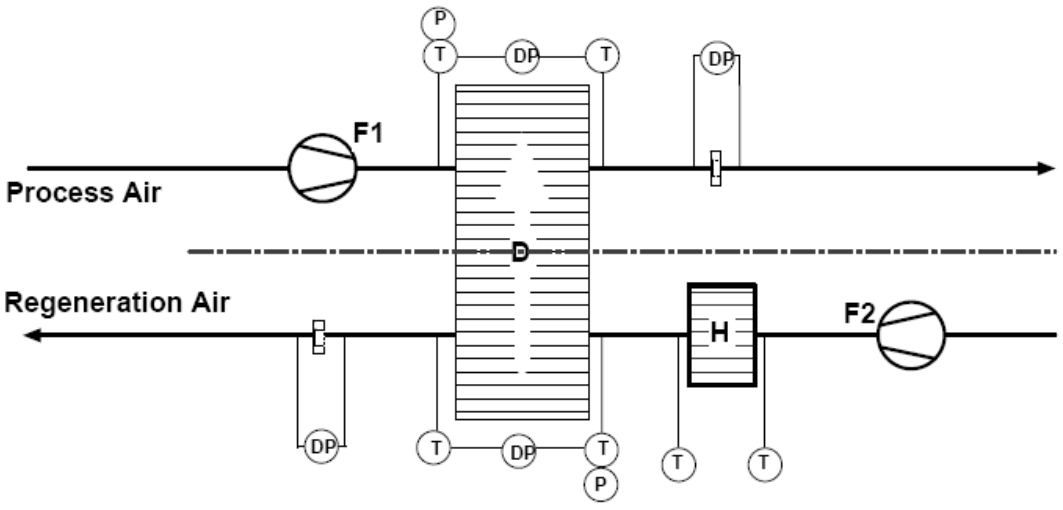

Figure 1: Schematic of experimental setup

Table 1: Specifications of LiCl wheel

Wheel mass (kg)	3.0	Wheel length (m)	0.25
Wheel Diameter (m)	0.4	Channel hydraulic diameter (mm)	1.44
Folio thickness (mm)	0.12	Wave height (mm)	2.0
Wavelength (mm)	4.0	Heat transfer area to volume ratio (m^2/m^3)	1360
Density (kg/m^3)	635	Specific heat of LiCl ($kJ\ kg^{-1}\ K^{-1}$)	3.0

For process air, the temperature at the inlet of the LiCl wheel is measured at the center of the duct. For the regeneration air, the inlet temperature is measured at the center, top and bottom of the duct. This is made to check the condition of uniform temperature at the inlet of the LiCl wheel. In order to evaluate the bulk temperature at the wheel exit, the exit air temperatures are measured at different locations as shown in Fig. (2). To perform an energy balance around the electric heater, the temperatures were also measured at the inlet and outlet of the electric heater; one location at the inlet and three locations at the outlet. The pressures at the inlet of the process and regeneration sections of the LiCl wheel are measured using pressure transmitters (Type: DMP 331). The pressure drop at each section of the LiCl wheel is measured using a differential pressure transmitter (Type: DP-10), manufactured by WIKA. The air volumetric flow rate is measured via an orifice plate. The orifice plate and its location are constructed in accordance with the DIN EN ISO 5167-2 standard. The pressure drop across the orifice plate is measured using a DP-10 differential pressure transmitter, in the range of 0-10 mbar. For the count of the number of revolution per minute (rpm), a magnetic sensor is installed at the external of the wheel.

The relative humidity is measured directly at four locations (inlet and outlet of the air regeneration and air process sections). The relative humidity meter is type EFK-E1S manufactured by *Kobold*. At the inlet of both sections the relative humidity is measured 10 cm away of inlets. At the outlet where the relative humidity is expected to be none uniformly distributed. The relative humidity is measured at 6 m away from the outlets. This is made to ensure uniform relative humidity distribution at the point of measurement. The corresponding dry-bulb temperatures are measured as well to facilitate the calculation of the humidity.

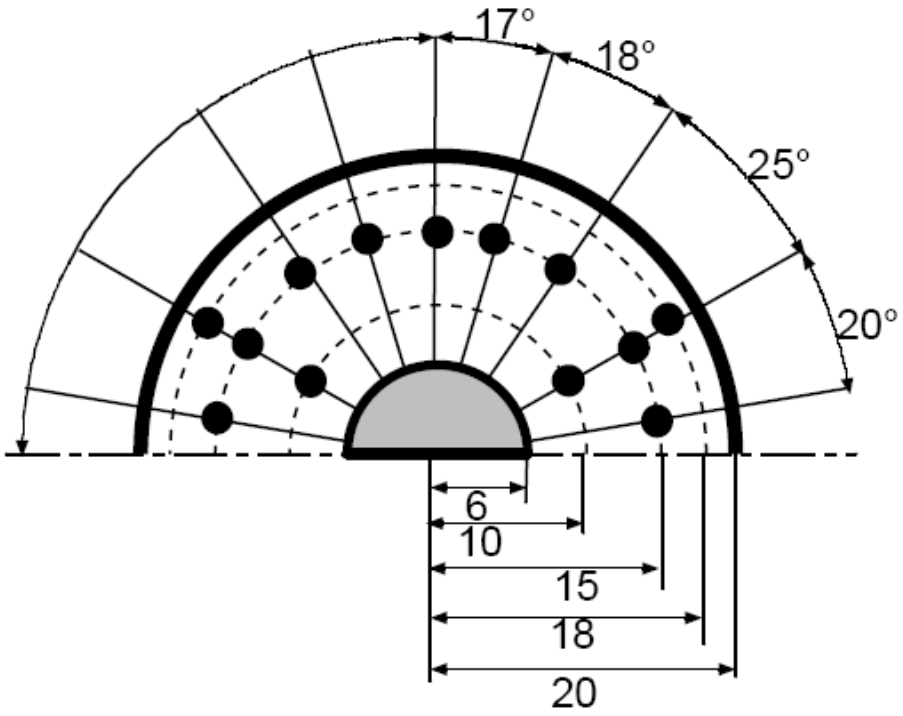

Figure 2: Temperatures measurement grid (dimensions in cm)

The measurement is facilitated with a data acquisition system running the software Labview version 8.5. The measurement system consists of a 40-channel Keithey multimeter type 2700 with a GPIB cable and a card. More details on the experimental setup are found in Rabah et al. [12].

3 Measurements and Uncertainties

Figure 1 shows the location where airflow temperature, pressure, pressure drop and relative humidity are measured. Figure 2 shows the location of the airflow temperature measurement at exits of the desiccant wheel. The volumetric airflow is measured via an orifice plate. The orifice plate and its location are constructed in accordance with the DIN EN ISO 5167-2 standard. The pressure drop across the orifice plate is measured using a differential pressure transmitter.

All sensors are calibrated and the combined uncertainty U is determined as

$$U = \sqrt{U_{inst}^2 + U_{cal}^2 + U_{rand}^2} \quad (1)$$

where U_{inst} is the instrumentation error, U_{cal} is the calibration error, which is the error of the reference device and U_{rand} is the random or precision error which is defined in accordance with Deutsche Kallibriendienst (DKD) as

$$U_{rand} = \frac{t_{\lambda,95\%}\sigma}{\sqrt{N}} \quad (2)$$

where t is the student test at a 95% confident interval, σ is the standard deviation, N is the number of data points and λ is the degree of freedom $\lambda = N - 1$.

Illustration 1: *The K-Type thermocouple is calibrated against a standard platinum resistance thermometer (SPRT) of type PT25. SPRT is calibrated by the 'Physikalisch Technischen Bundesanstalt (PTB)' to an uncertainty of 2.0-4.0 mK in the temperature range of 0-120* °C. *For the purpose of calibration both the thermometer and SPRT are placed in a thermostat in which a copper block calibrator is immersed. For all thermocouples employed in this work, a level of uncertainty in the range of 0.10 - 0.25 K is realized. This range is equivalent to 0.5-1.0% for the temperature range of 20 - 70* °C*; where 20* °C *is the average room temperature during the measurement and 70* °C *is the maximum regeneration temperature used in this work.*

For a parameter that is not directly measured such as airflow rate and absolute humidity ratio, the uncertainty is calculated using the law of propagation of error. For example if the parameter y is a function of variables x's as

$$y = f(x_1, x_2, x_3, ...) \quad (3)$$

The uncertainty $U(y)$ is

$$U(y) = \left\{ \sum \left[c(x)U(x) \right]^2 \right\}^{0.5} \tag{4}$$

Where $U(x)$ and $c(x)$ are the uncertainty and the sensitivity coefficient of the variable x respectively. The sensitivity coefficient is defined as

$$c(x) = \frac{\partial y}{\partial x} \tag{5}$$

Illustration 2*: To measure the volumetric airflow the orifice flow equation is used*

$$\dot{V} = C_d A_n Y \sqrt{\frac{2\Delta P}{\rho\left(1-\beta^4\right)}} \tag{6}$$

where V is the volumetric airflow, C_d is the orifice discharge coefficient, A is the area at the orifice exit, ΔP is the measured pressure drop across the orifice, Y is the expansion factor, ρ is the air density at the upstream of the orifice $\beta = d/D$ is the contraction ratio and d and D are the orifice and the duct diameter respectively. With only ΔP and ρ are variables, the uncertainty in the airflow rate in according with eq. (4) is

$$\frac{U\left(\dot{V}\right)}{\dot{V}} = \sqrt{\left[\frac{U\left(\Delta P\right)}{2\Delta P}\right]^2 + \left[\frac{U\left(\rho\right)}{2\rho}\right]^2} \tag{7}$$

Table (2) shows the uncertainty level of the measurement devices, the manufacturer's uncertainty is also given.

Table 2: Measurement range and uncertainty

Parameter	Range	Uncertainty		
		Manufacturer	**this work**	**Unit**
Temperature [°C]	-10 …100	*0.05+0.01T*	0.10 … 0.25	K
Pressure [bar]	0 …1.6	0.25	0.15	%
Differential Pressure [mbar]	0 … 19.99	1.0	0.5	%
Wheel speed [rpm]	0 … 24	NA	0.1 … 0.2	%
φ [%]	0 …100	$1.5+0.015\varphi$	1.0	%
M [kg/h]	100 … 500		1.0	%
W [g/kg]	0.0 … 20.0		1.0	%

4 Data reduction

4.1 Performance factors and indices

In accordance with ANSI/ASHRAE [2] there are many performance factors and indices of the desiccant wheel. In this work the COP and sensible effectiveness is considered. The COP reflects the dehumidification capacity and energy input at the same time, wheras the sensible effectiveness represents the heat exchange between the process and regeneration air.

The sensible effectiveness is defined, assuming a constant specific heat, as

$$\varepsilon = \frac{C_p\left(T_{po} - T_{pi}\right) + C_r\left(T_{ri} - T_{ro}\right)}{2C_{\min}\left(T_{ri} - T_{pi}\right)} \tag{8}$$

where the subscripts p and r stand for process and regeneration airflow respectively and $C = MC_p$ is the heat capacity. For constant air properties and a uniform velocity, the bulk airflow temperatures at the exit of the process air, for example, is calculated as

$$T_{po} = \frac{\int_0^{\pi}\int_0^{R} T_{po}(r,\theta) r dr d\theta}{\int_0^{\pi}\int_0^{R} r dr d\theta} \tag{9}$$

The integration given by eq. (9) under the assumption of a constant volumetric flow rate is evaluated numerically as

$$T_{po} = \frac{1}{N}\sum\sum T_{po,ij} \tag{10}$$

where *i* stands for *r*, j for μ, $T_{po,ij} = T_{po}(r,\theta)$ and N is the number of measurement nodes shown in Fig. 2.

- Coefficient of performance(COP) for latent cooling

$$COP = \frac{MRC\Delta h_v}{E_r + E_{para}} \tag{11}$$

where Δh_v is the moisture latent heat of condensation, MRC moisture removal capacity, E_r is the regeneration thermal energy input and E_{para} is the parasitic energy. Parasitic energy input includes the drive motor used to rotate the wheel and the fan power required to overcome the pressure drops through the process and regeneration sides of the wheel. The parasitic energy input is not considered in this work. The MRC is defined as

$$MRC = \dot{M}_p\left(W_{po} - W_{pi}\right) \tag{12}$$

where *W* is the absolute humidity ratio. The regeneration thermal energy is

$$E_r = C_r\left(T_{ri} - T_o\right) \tag{13}$$

where T_o is the ambient temperature.

4.2 Dimensionless Group

The sensible effectiveness analogous to heat exchanger is generally characterized by the dimensionless groups of airflow heat capacity ratio (C^*), the matrix heat capacity ratio (Cr^*), and the number of transfer units (NTU). These dimensionless groups are defined as:

- The airflow heat capacities ratio

$$C^* = \frac{C_{\min}}{C_{\max}} \tag{14}$$

where

$$C_{\min} = \min\left(C_r, C_p\right) \tag{15}$$

$$C\max = \max\left(C_r, C_p\right) \tag{16}$$

For balanced flow $C^* = 1$.

- Matrix capacity ratio

$$Cr^* = \frac{C_m}{C_{\min}} \tag{17}$$

Where

$$C_m = M_m C_{pm} \omega \tag{18}$$

where C_{pm} is the specific heat capacity of the matrix, M_m is the mass of the matrix in kg and ω is the rotational speed. The mass of the matrix is $M_m = \rho_m V$, where ρ is desiccant density and V is the solid volume of the matrix.

- The number of heat transfer unit is

$$NTU = \frac{UA}{C_{\min}} \tag{19}$$

Where

$$\frac{1}{UA} = \frac{1}{h_p A_p} + \frac{1}{h_r A_r} \tag{20}$$

Prior to the analysis of the results, the influence of measurement uncertainties in the effectiveness and COP are estimated. Based on the uncertainty of the sensors given in section 2 the propagated uncertainty is within ±2% for effectiveness, ±3% for COP for wide range of operation conditions.

Table 3: Operation conditions

Parameter	Range	
	Min	Max
T_r	50	70
φ_o	30	65
T_o	18	28
M	290	530
C^*	0.94	1.00
Cr^*	0.05	8.98
Crm^*	0.05	10.04
NTU	3.83	7.13
COP	0.00	0.47
ε	0.20	0.84
T_r=Regeneration temperature [°C]		
φo=Ambient relative humidity [%]		
T_o=Ambient air temperature [°C]		
M=Airflow rate [kg/h]		

5 Results and Discussion

The experimental results include 10 test runs constituting of about 130 data points covering a wide range of operating conditions. The results are presented in Tab. A.1 to A.2. Tab. 3 gives the range of operating conditions and the performance factors for all data points.

5.1 Rotational speed

Figure 3 shows the influence of rotational speed on sensible effectiveness and COP. The effectiveness initially increases sharply with the rotational speed till it reaches a critical point, then remains constant. This implies that the maximum sensible effectiveness of the LiCl wheel can be obtained at a lower rotational speed of 2 rpm. Lowering the power consumption to a level that can be supplied by a solar panel will make grid-independent solar desiccant air conditioning systems possible.

As shown in Fig. 3 the rotational speed has strong influence on COP as well. COP peaks at a very low rotational speed of about 0.2 rpm (12 rph). Beyond this rotational speed the COP drops before it asymptotes to a constant value at about 4 rpm. The occurrence of the maximum COP at a low rotational speed is expected. If the rotational speed is too high the desiccant cannot fully adsorb or desorb water molecules because of the short process time. Since the main purpose of the desiccant wheel is to remove humidity rather than exchanging heat, the rotational speed that yields the maximum COP is recommended. The numerical work of Ge et al [8] recommended an optimum speed of 12 rph.

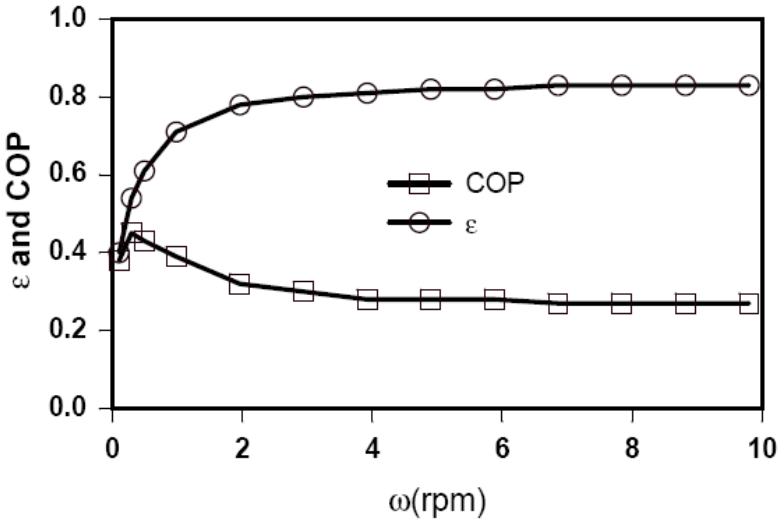

Figure 3: Influence of rotational speed on ε and COP (M =310 kg/h, T_r =50 °C)

5.2 Regeneration temperatures

Figures (4a) presents the variation of effectiveness with rotational speed for various regeneration temperatures at a constant mass flow rate. Analogous to sensible heat exchangers, it is expected that the effectiveness of the LiCl wheel to be independent of regeneration temperatures. Visual inspection of Fig. 4a confirms this expectation; there is no significant variation in effectiveness with regeneration temperatures. The physical justification to this is that the specific heat capacities of the LiCl and the air are almost constant for a wide range of temperatures. For example the specific heat capacity of air varies between 1 kJ kg^{-1} K^{-1} and 1.012 kJ kg^{-1} K^{-1} in the temperature range of 0°C to 100 °C [14]. Figure (4b) shows the influence of regeneration temperature on COP. It is clear that COP depends strongly on the regeneration temperatures and it decreases as regeneration temperature increases. On the contrary, this is not expected since a high regeneration temperature speeds up moisture removal. However, high regeneration temperatures will dry-up the wheel before it completes the regeneration period. Hence part of the energy added will not be utilized in moisture removal. On the other hand it seems that the amount of the energy needed to produce the high regeneration temperature overweighs the actual energy used for moisture removal [8]. A low regeneration temperature enhances the potential of LiCl to solar application.

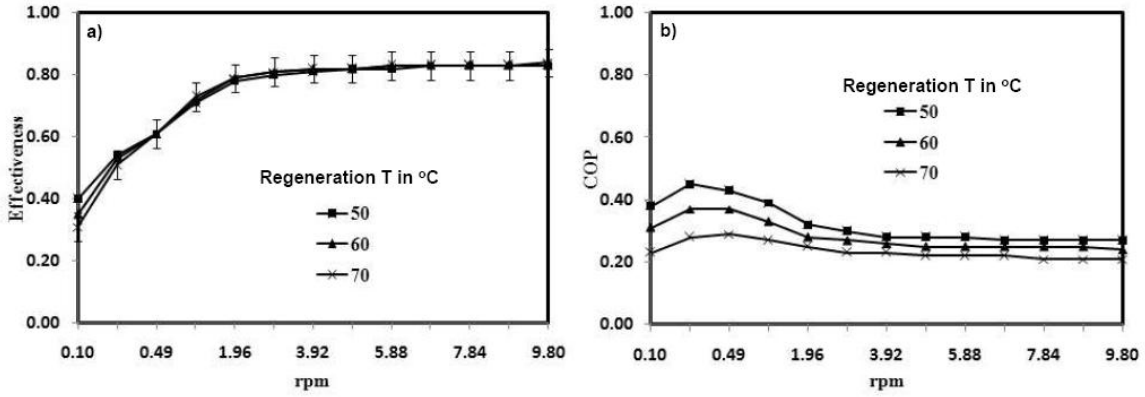

Figure 4: Influence of regeneration temperature on (a) effectiveness (b) COP. Mass flow rate is 310 kg/h. The error bars are at 95% confidence limit

5.3 Mass flow rate

The mass flow rate is an important parameter in the design of the desiccant wheels. However, most of the desiccant wheels used in HVAC operate at a balance flow (C^*=1) condition. This is due to the fact that leakages between the streams are inevitable, and as such an unbalanced flow is difficult to maintain. Figure 5a shows the dependency of effectiveness on airflow rate for various rotational speeds at a constant regeneration temperature. The influence of airflow rate in effectiveness is insignificant in the range of operation rotational speed (at maximum effectiveness). This is attributed to the fact that a high airflow rate increases the heat transfer coefficient slightly.

Figure 5b shows the influence of airflow rate on COP. The COP decreases with increasing airflow rate. High airflow rates at both sides of the wheel mean more energy is available for regeneration and also more moisture input to the wheel. However, the desiccant adsorption capacity is constant and as such the moisture removal capacity per unit of mass of process air decreases with increasing airflow rate. Since the flow is balanced and regeneration and ambient conditions are constant, in accordance with eq. (11) the decrease of COP with airflow rate is justified.

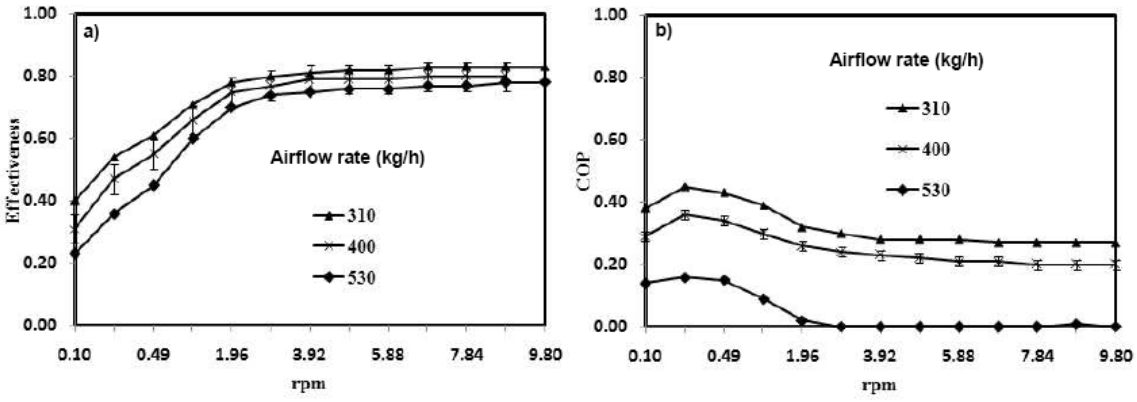

Figure 5: Influence of mass flow rate on (a) effectiveness (b) COP. Regeneration temperature is 50 ℃. Error bars are at 95% confidence limit

5.4 Comparison with correlation

The experimental results are compared with the available correlations for the prediction of effectiveness in particular Kays and London [15]. The general form of the correlation is

$$\varepsilon = \varepsilon_o F \tag{21}$$

where F is a correction factor and ε_o is the effectiveness of counter-current heat exchanger which is

$$\varepsilon_o = \begin{cases} \dfrac{1-\exp\left(-\left(1-C^*\right)NTU\right)}{1-C^*\exp\left(-\left(1-C^*\right)NTU\right)} & C^* < 1 \\ \dfrac{NTU}{1+NTU} & C^* = 1 \end{cases} \tag{22}$$

The correction factors is defined as

$$F = 1 - \frac{1}{7.5 Cr^{*}} \tag{23}$$

The correlation is valid at $2 < NTU < 14$ and $Cr^{*} < 2$.

To compare the correlation and experimental data, numerous quality measurements based on statistical error analysis are computed. These include percent deviation (PD), average absolute percent deviation (AAPD), minimum absolute percent deviation (APD_{min}) and maximum absolute percent deviation (APD_{max}). The percent deviation is defined as

$$PDi = \frac{\varepsilon_{\exp,i} - \varepsilon_{calc,i}}{\varepsilon_{\exp,i}} \tag{24}$$

where $\varepsilon_{exp;i}$ and $\varepsilon_{calc,i}$ are the experimental and calculated effectiveness respectively.

Tables A.1 and A.2 show the experimental results for different test runs (coded A to K). For each test run ω, C^{*}, Cr^{*}, NTU, ε_{exp}, PD_i are provided. It should be highlighted that PD is given only for data that falls within the applicability range of the correlation. The blank cells in Tab. A.1 and A.2 are for data that fall outside the range of the correlation.

Table 4 summaries the range of operation conditions and statistical parameters for all test runs. The correlation predicts the experimental data for all test runs, with a grand AAPD of 2.16 and APD_{max} of about 6.00. It can be concluded that, despite the fact that the correlation is developed for molecular sieve and silica gel wheels the correlation is also valid for LiCl wheel.

Table 4: Summary of operating conditions and statistical parameters

Run	***Tr*** (°C)	***M*[a]** (Kg/h)		***C**[a]** **(-)**	***Cr**** **(-)**		***NTU*** **(-)**		**ε (–)**			**Data**
		p	***r***		Min	Max	Min	Max	APD_{min}	APD_{max}	AAPD	Points
A	50	534.31	530.54	.99	0.05	4.78	3.83	3.99	0.29	3.16	1.16	13
B	60	531.38	527.54	0.99	0.05	4.81	3.90	4.02	0.58	3.07	1.39	13
C	70	524.85	521.92	0.98	0.05	4.90	3.92	4.07	1.32	3.52	2.19	13
D	50	310.46	311.54	.99	0.08	8.21	6.50	6.64	1.84	3.95	2.53	13
E	60	308.46	310.92	0.99	0.08	8.28	6.45	6.62	1.11	3.75	2.24	13
F	70	05.54	306.54	.99	0.08	8.33	6.53	6.76	0.14	2.87	2.04	13
G	50	89.31	289.23	.99	0.09	8.82	6.98	7.08	0.83	6.04	4.97	13
H	70	86.00	289.00	.98	0.09	8.98	6.94	7.13	0.70	4.32	3.28	13
I	50	403.08	399.08	0.99	0.06	6.32	5.09	5.24	0.49	1.72	1.19	13
K	70	96.83	396.83	0.98	0.06	6.53	5.11	5.32	0.08	2.21	0.60	13
Grand					0.05	8.98	3.83	7.13	0.08	6.04	2.16	130

[a] average
p=process air
r=regeneration air

6. Conclusion

Extensive experimental investigation of the performance of LiCl wheel is presented. The influence of operating conditions of rotational speed, regeneration temperature and airflow rate on the effectiveness and COP are studied. It is established that a maximum COP can be obtained at low rotational speed of about 12 rph. A lower rotational speed reflects a lower power consumption of the wheel motor. If the power consumption is lowered to a level that can be provided by a solar panel, a grid- independent solar desiccant air conditioning systems may be realized. The results also concluded that Kays and London correlation is sufficient in the prediction of the effectiveness of the LiCl wheel for wide range of operating conditions. The work also provides experimental data in a tabular form that may be useful to researchers in the field.

References

[1] Shang, W., Besant, R. W. (2004). Measurement of the Pore Size Variation and Its Effect in energy Wheel Performance. ASHRAE transaction, 110 (1), pp. 410-421.

[2] ARI, ANSI/ARI Standard 1060-2001. (2001). Standard for Rating Air-to-Air Heat Exchangers for Energy Recovery Ventilation Equipment. Air-Conditioning and Refrigeration
Institute, Arlington, VA.

[3] ANSI/ASHRAE. (2009). ANSI/ARI Standard 174-2009, Method of Test for Rating Desiccant-Based Dehumidifcation Equipment. American Society of Heating, Refrigerating and Air-Conditioning Engineers Inc. 1971 Tullie Circle NE, Atlatan, GA
30329

[4] Simonson, C. J., Besant, R. W. (1999). Energy Wheel Effectiveness: Part I Development of Dimensionless Groups. International Journal of Heat and Mass Transfer 42, pp. 2161-2170.

[5] Simonson, C. J., Besant, R.W. (1999). Energy Wheel Effectiveness: Part Ii-Correlations. International Journal of Heat and Mass Transfer 42, pp. 2171-2185.

[6] Simonson, C. J., Besant, R. W. (1997). Heat and Moisture Transfer in Desiccant Coated Rotary Energy Exchangers: Part I. Numerical Model. HVAC&R Research 3 (4), pp. 325-350.

[7] Simonson, C. J., Shang, W., Besant, R. W. (2000). Part Load Performance of Regenerative Heat Exchanger Effectiveness: Part Ii-. by Pass Control and Correlation. ASHRAE transaction 106(1), pp. 301-310.

[8] Ge, T. S., Ziegler, F., Wang, R. Z. (2010). A Mathematical Model for Predicting the Performance of a Compound Desiccant Wheel (A Model for Compound Desiccant Wheel). Applied Thermal Engineering 30, pp.1005-1015

[9] Xuan, S., Radermacher, R. (2005). Transient Simulation for Desiccant and Enthalpy Wheels. International Sorption Heat Pump Conference June 22-24, Denver, CO, USA ISHPC-098-2005.

[10] Zheng, W., and Worek, W.M. (1993). Numerical Simulation of Combined Heat and Mass Transfer Processes in a Rotary Dehumidifier. Numerical Heat Transfer 23(A): pp. 211-232.

[11] Rabah, A. A.; Mohamed, S. A. (2009). Latent Effectiveness of Desiccant Wheel: A Silica Gels-Water System, Journal of Industrial Research. 6, pp. 12-22.

[12] Rabah, A. A.; Fekete, A.; Kabelac, S. (2009). Experimental Investigation on a Regenerator
Operating at Low Temperatures. ASME Journal of Thermal Sciences and Engineering Applications, 1 (4), pp. 041004-13.

[13] Shah, R. K. (1981). Thermal Design Theory of LiCl Wheels. In: Kakac, S., Bergles, A. E., Mayinger, F., 1981, Heat Exchangers: Thermal-Hydraulic Fundamentals and Design, pp. 721-763, Hamisphere, New York.

[14] VDI, VDI-GVC. (2007). VDI- Waermeatlas, 10. Aufl., Springer-Verlag, Berlin.

[15] Kays, W. M., London, A. L. (1984). Compact Heat Exchangers. McGraw-Hill, New York.

Nomenclature

A	Heat transfer area [m^2], Constant [-]
Cp	Specific heat capacity [J $kg^{-1}k^{-1}$]
˙C	Heat capacity [W $°C^{-1}$]
E	Energy [W]
F	Correction factor[-]
h	Heat transfer coefficient[W $m^{-2}°C^{-1}$]
M	Mass flow rate [kg/h]
r	Radius [m]
T	Temperature [°C]
U	Uncertainty[-]
V	Matrix volume [m^3]
˙V	Volumetric airflow [m^3/h]
W	Humidity ratio [-]
Greek Symbols	
λ	Thermal conductivity [J $kg^{-1}K^{-1}$], Degree of freedom[-]
ρ	Density [kgm¡3]
φ	Relative humidity[-], Effectiveness correction factor[-]
ε	Effectiveness [-]
ω	Rotational speed[rad]
Dimensionless parameters	
C^*	Heat capacity ratio[C_{min}/C_{max}]
Cr^*	Matrix to airflow heat capacity ratio[Cr/C_{min}]
COP	Coefficient of performance [-]
MRC	Moisture removal capacity [-]
NTU	Number of transfer units [hA/C_{min}]
Subscripts	
i	Inlet, Index
m	Matrix
max	Maximum
min	Minimum
o	Exit, Ambient
p	Process
r	Regeneration
Superscripts	
°	Degree

Table A.1: Experimental data of test runs A to F.

rpm	C^*	Cr^*	NTU	ε	PD	C^*	Cr^*	NTU	ε	PD
	A					*B*				
0.10	0.98	0.05	3.83	0.23		0.98	0.05	3.90	0.20	
0.29	0.96	0.14	3.99	0.36		0.96	0.15	4.02	0.34	
0.49	0.97	0.24	3.98	0.45		0.97	0.24	4.00	0.44	
0.98	0.98	0.48	3.96	0.60	3.16	0.98	0.49	3.98	0.60	3.07
1.96	0.99	0.96	3.95	0.70	1.93	0.99	0.97	3.96	0.70	2.37
2.94	0.99	1.44	3.93	0.74	1.66	1.00	1.44	3.93	0.74	1.80
3.92	1.00	1.92	3.93	0.75	1.36	1.00	1.92	3.93	0.75	1.41
4.90	1.00	2.40	3.93	0.76	1.00	1.00	2.41	3.94	0.76	1.28
5.88	1.00	2.87	3.92	0.76	0.63	1.00	2.89	3.94	0.77	1.03
6.86	1.00	3.35	3.92	0.77	0.58	1.00	3.37	3.94	0.77	0.85
7.84	1.00	3.84	3.92	0.77	0.47	0.99	3.85	3.94	0.78	0.84
8.82	1.00	4.31	3.92	0.78	0.50	1.00	4.33	3.94	0.78	0.70
9.80	1.00	4.78	3.92	0.78	0.29	1.00	4.81	3.94	0.78	0.58
	C					*D*				
0.10	0.98	0.05	3.92	0.20		0.99	0.08	6.58	0.40	
0.29	0.94	0.15	4.07	0.32		0.99	0.25	6.64	0.54	
0.49	0.96	0.25	4.05	0.42	0.99	0.41	6.60	0.61	3.95	
0.98	0.98	0.49	4.04	0.61	3.52	1.00	0.82	6.50	0.71	-1.96
1.96	0.99	0.98	4.00	0.72	3.45	0.99	1.64	6.52	0.78	-1.84
2.94	1.00	1.46	3.99	0.75	2.79	0.99	2.46	6.52	0.80	-1.91
3.92	0.99	1.95	3.99	0.76	2.34	0.99	3.27	6.51	0.81	-2.15
4.90	0.99	2.45	4.00	0.77	2.09	0.99	4.09	6.52	0.82	-2.43
5.88	0.99	2.94	4.01	0.78	1.92	0.99	4.91	6.51	0.82	-2.55
6.86	0.99	3.43	4.00	0.78	1.62	0.99	5.74	6.53	0.83	-2.59
7.84	0.99	3.92	4.01	0.78	1.41	0.99	6.56	6.53	0.83	-2.78
8.82	0.99	4.41	4.01	0.79	1.32	0.99	7.38	6.53	0.83	-2.79
9.80	0.99	4.90	4.01	0.79	1.40	0.99	8.21	6.54	0.83	-2.88
	E					*F*				
0.10	1.00	0.08	6.45	0.35		0.99	0.08	6.53	0.31	
0.29	0.98	0.25	6.62	0.53		0.97	0.25	6.76	0.51	
0.49	0.99	0.41	6.57	0.61	3.75	0.98	0.42	6.70	0.61	1.75
0.98	1.00	0.82	6.56	0.72	-1.11	0.99	0.84	6.65	0.73	-0.14
1.96	0.99	1.65	6.58	0.79	-1.58	1.00	1.67	6.64	0.79	-1.28
2.94	0.99	2.48	6.58	0.81	-1.75	0.99	2.50	6.64	0.81	-1.68
3.92	0.99	3.31	6.58	0.82	-1.85	0.99	3.34	6.65	0.82	-2.05
4.90	0.98	4.14	6.59	0.82	-2.06	0.99	4.18	6.66	0.82	-2.31
5.88	0.99	4.96	6.58	0.83	-2.34	0.99	5.01	6.65	0.83	-2.56
6.86	0.98	5.80	6.60	0.83	-2.37	0.99	5.85	6.64	0.83	-2.64
7.84	0.98	6.62	6.59	0.83	-2.54	0.99	6.69	6.65	0.83	-2.87
8.82	0.98	7.46	6.60	0.83	-2.60	0.99	7.54	6.66	0.83	-2.79
9.80	0.98	8.28	6.59	0.83	-2.64	0.98	8.33	6.63	0.84	-2.39

Table A.2: Experimental data of test runs G to K.

rpm	C^*	Cr^*	NTU	ε	PD	C^*	Cr^*	NTU	ε	PD
	G					*H*				
0.10	0.99	0.09	6.98	0.38		0.99	0.09	6.94	0.37	
0.29	0.97	0.26	7.08	0.53		0.97	0.26	7.02	0.51	
0.49	0.99	0.44	7.03	0.61	-0.83	0.98	0.44	7.04	0.61	-0.70
0.98	0.99	0.88	7.01	0.71	-4.10	1.00	0.89	7.07	0.73	-2.26
1.96	1.00	1.76	6.99	0.77	-4.62	0.98	1.79	7.10	0.79	-2.70
2.94	1.00	2.64	6.98	0.79	-4.93	0.98	2.69	7.12	0.81	-3.01
3.92	1.00	3.52	6.99	0.80	-5.20	0.98	3.59	7.12	0.82	-3.33
4.90	0.99	4.41	6.99	0.80	-5.61	0.98	4.49	7.12	0.82	-3.52
5.88	0.99	5.29	6.99	0.81	-5.71	0.98	5.39	7.13	0.82	-3.80
6.86	0.99	6.17	7.00	0.81	-5.80	0.98	6.28	7.12	0.82	-4.07
7.84	0.99	7.06	7.00	0.81	-5.93	0.98	7.18	7.12	0.83	-4.15
8.82	0.99	7.93	6.99	0.81	-6.04	0.98	8.06	7.11	0.83	-4.25
9.80	0.99	8.82	7.00	0.81	-5.91	0.98	8.98	7.12	0.83	-4.32
	I					*K*				
0.10	0.98	0.06	5.11	0.31		0.99	0.06	5.11	0.27	
0.29	0.96	0.19	5.24	0.47		0.95	0.20	5.32	0.43	
0.49	0.97	0.32	5.20	0.55		0.98	0.32	5.17	0.53	
0.98	0.98	0.64	5.20	0.66	-0.55	1.00	0.64	5.13	0.68	2.21
1.96	0.99	1.27	5.12	0.75	-0.49	1.00	1.29	5.19	0.76	0.44
2.94	0.99	1.90	5.12	0.77	-0.55	0.99	1.93	5.18	0.79	0.77
3.92	0.99	2.54	5.13	0.79	-0.98	0.98	2.57	5.18	0.79	-0.75
4.90	0.99	3.18	5.12	0.79	-1.25	0.99	3.23	5.20	0.80	0.08
5.88	0.99	3.81	5.12	0.79	-1.72	0.99	3.88	5.21	0.81	-0.29
6.86	1.00	4.44	5.11	0.80	-1.55	0.98	4.56	5.25	0.82	0.39
7.84	0.99	5.08	5.12	0.80	-1.62	0.98	5.23	5.26	0.82	0.28
8.82	1.00	5.68	5.09	0.80	-1.56	0.98	6.53	5.26	0.82	0.21
9.80	1.00	6.32	5.10	0.81	-1.66	0.98	6.53	5.26	0.82	0.21